



## INDIVIDUAL PROJECT REPORT

IMPERIAL COLLEGE LONDON

DEPARTMENT OF COMPUTING

---

# Tackling Crohn's Disease using Deep Learning

---

*Author:*  
Feifan Fan

*Supervisor:*  
Dr. Bernhard Kainz  
*Second Marker:*  
Prof. Ben Glocker

Submitted in partial fulfilment of the requirements for the MEng  
Mathematics and Computer Science of Imperial College London

## Abstract

Crohn’s disease is a severe inflammatory bowel disease without a cure. Early diagnosis via T2-weighted MRI scanning of the terminal ileum can significantly improve patient outcomes. To facilitate this, we developed an enhanced segmentation model based on prior work to improve diagnostic accuracy. We used the SegmentAnything Model (SAM) from Meta AI and adapted it to a two-stage training process due to limited human-annotated segmentations. In the first stage, we employed a MedSAM variant to create a refined weak mask from bounding box information derived from centerline coordinates. This enabled us to build a proxy model using nnU-Net in 2D and 3D full-resolution configurations. The second stage involved training this model on fully annotated data. A rigorous 5-fold cross-validation process validated our model. We further identified the best-performing model using an ensemble method across various configurations and folds. Our approach showed superior performance in weak label generation and segmentation compared to previous studies, leading to improved Dice Similarity Coefficient metrics. Our results confirm the potential of pre-trained models and suggest that higher-quality weak labels could significantly enhance segmentation outcomes. This study brings us closer to more effective Crohn’s disease management strategies, indicating promising results with small datasets and nuanced multi-class segmentation differentiating between normal and abnormal terminal ileum tissues.

## Acknowledgements

I wish to express my deepest gratitude to my supervisor and long-standing mentor, Dr Bernhard Kainz. His dynamic guidance, free of excessive constraints, allowed me to navigate my research path boldly and innovatively. The insightful feedback he patiently provided on my inquiries has been instrumental in this journey. The success of this project and the immense learning it presented would not have been possible without Dr Kainz's unwavering support.

My heartfelt appreciation extends to my neighbour, knowledgeable colleague, and self-proclaimed "charming" friend, Tiansheng Xu. With his consistent presence and support, Tiansheng has enriched both the challenging and joyful moments throughout my final year, helping make it a truly memorable experience.

I hold a profound respect for my old friend, Michael Wen. As an adept engineer and culinary maestro, Michael has been a fountainhead of fresh perspectives and gourmet delicacies that have only brightened my journey. Having achieved significant success as a UCL graduate, I am confident his academic voyage at Cambridge will be equally triumphant. In the same vein, I sincerely thank all the friends who have stood by me during this endeavour. Your support has been the beacon guiding my way.

Most importantly, I dedicate this achievement to my loving family: my pillars of strength, Yunjia Zhou and Junhua Fan. Their unwavering trust and belief in my abilities are the foundational stones of my success. They have shared my joys, extended their assistance in times of difficulty, and instilled in me a profound sense of self-assurance. My parents' pride in my accomplishments is my greatest honour. We often quote, "The last one is the best one," and today, I dedicate this final, best victory to them in this very last but important paragraph. This milestone would not have been attainable without their unconditional love and support.

# Contents

<b>List of Figures</b>	<b>3</b>
<b>1 Introduction</b>	<b>4</b>
1.1 Crohn’s Disease . . . . .	4
1.2 Motivation . . . . .	5
1.3 Machine Learning Challenges . . . . .	6
1.4 Objectives . . . . .	6
<b>2 Background</b>	<b>8</b>
2.1 Delving into Image Segmentation . . . . .	8
2.2 Manual Segmentation . . . . .	9
2.3 Region-based Methods . . . . .	9
2.4 Deep Learning Methods . . . . .	10
2.4.1 U-Net: An Automated Deep Learning Method for Image Segmentation . . . . .	10
2.4.2 nnU-Net: A Self-configuring Framework Aligned with Our Research Goals . . . . .	11
2.5 Generating Weak Labels: A Strategic Response to Annotation Scarcity . . . . .	12
2.5.1 Leveraging Unsupervised Methods: Simple Linear Iterative Clustering (SLIC) . . . . .	13
2.5.2 Harnessing Pretrained Models: The Segment Anything Model (SAM) . . . . .	14
<b>3 Related Work</b>	<b>15</b>
3.1 Automatic Detection and Segmentation of Crohn’s Disease Tissues from Abdominal MRI . . . . .	15
3.2 Automatic Detection of Bowel Disease with Residual Networks	16
3.3 Leveraging Machine Learning Methods for Accurate Prediction of Intestinal Damage in Crohn’s Disease Patients . . . . .	17
<b>4 Ethical Discussion</b>	<b>18</b>

<b>5</b>	<b>Dataset Analysis</b>	<b>19</b>
5.1	Dataset Exploration . . . . .	19
5.2	Dataset Specification . . . . .	20
5.3	Ground Truth Segmentations . . . . .	21
<b>6</b>	<b>Methodology</b>	<b>23</b>
6.1	Dataset Preprocessing . . . . .	23
6.2	Baseline Implementation . . . . .	24
6.3	Model Training . . . . .	24
6.3.1	Refining Weak Masks with MedSAM . . . . .	25
6.3.2	Executing Dataset Partitioning . . . . .	26
6.3.3	Establishing the Training Pipeline . . . . .	26
6.3.4	Executing the Inference Process . . . . .	30
<b>7</b>	<b>Evaluation</b>	<b>32</b>
7.1	Evaluation metric . . . . .	32
7.1.1	Dice Similarity Coefficient (DSC) . . . . .	32
7.1.2	Jaccard Similarity Coefficient . . . . .	33
7.1.3	Hausdorff Distance . . . . .	34
7.2	Evaluation Method . . . . .	34
7.2.1	Employing Dice Similarity Coefficient for Qualitative Evaluation . . . . .	34
7.2.2	Utilizing the t-Test for Evaluating Statistical Significance . . . . .	34
7.3	Evaluation Plan . . . . .	35
<b>8</b>	<b>Results</b>	<b>37</b>
8.1	Weak Label generation . . . . .	37
8.1.1	Visual Validation of Model Performance . . . . .	38
8.1.2	Statistical Evaluation for Establishing Significance . . . . .	39
8.2	T.I. Segmentation . . . . .	40
8.2.1	Visual Validation of Model Performance . . . . .	41
8.2.2	Statistical Evaluation for Establishing Significance . . . . .	41
8.3	Ablation Studies . . . . .	43
<b>9</b>	<b>Conclusion and Future Work</b>	<b>46</b>
9.1	Conclusion . . . . .	46
9.2	Future Work . . . . .	47
	<b>Bibliography</b>	<b>49</b>

# List of Figures

1.1	The gastrointestinal tract of a Human . . . . .	4
2.1	Different Image Segmentation Tasks . . . . .	8
2.2	An example of the U-net architecture. . . . .	10
2.3	The pipeline representation of nnU-Net. . . . .	12
2.4	Superpixel Segmentation using SLIC . . . . .	13
5.1	T2-Weighted MRI with different modalities in the dataset . .	20
5.2	Detailed breakdown of segmentation specifics and label distribution across diverse categories of image data . . . . .	21
6.1	Nesterov momentum . . . . .	28
8.1	A Cross-Model Comparison between Ground Truth and Generated Weak Masks . . . . .	39
8.2	Comparative Segmentation Performance Analysis . . . . .	42
8.3	Effect of T.I. Localisation on Mask Generation . . . . .	44

# Chapter 1

## Introduction

### 1.1 Crohn's Disease

Crohn's Disease [1, 2] is one of the primary types of Inflammatory Bowel Disease (IBD) [3]. It is characterised by its chronic nature with inflammation in the gastrointestinal (GI) tract (indicated in Figure 1.1 [4]). This condition can lead to long-term damage and complications, such as strictures, fistulas, and abscesses. Many people worldwide struggle with IBD, and the management remains challenging for medical professionals to address. A study from the University of Nottingham [5] reports that more than half a million individuals in the UK are affected by Crohn's Disease and Ulcerative Colitis, another significant IBD subtype.

Unlike Ulcerative Colitis, which is limited to the colon and rectum, Crohn's disease can potentially develop lesions anywhere within the GI tract. Consequently, patients may experience diverse symptoms, including abdominal pain, diarrhoea, fatigue, and weight loss.

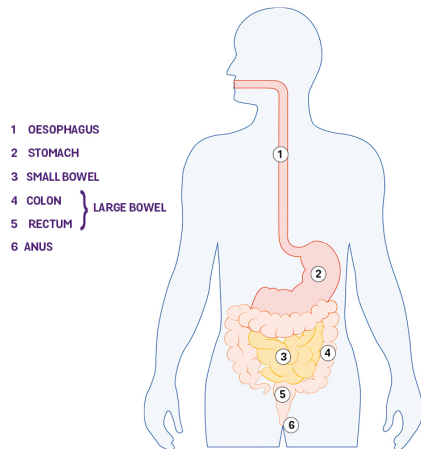


Figure 1.1: The gastrointestinal tract of a Human

Although numerous research initiatives have been undertaken [6, 7], the precise cause of Crohn’s disease is still not wholly understood, rendering it incurable. However, fortunately, early diagnosis and appropriate treatment can alleviate patients’ symptoms and substantially improve their quality of life. Various diagnostic methods are employed by clinicians, such as enteroclysis, endoscopy, colonoscopy, and radiographic techniques (including barium contrast X-rays, Computed Tomography (CT), and Magnetic Resonance Imaging (MRI)) to assist in the early diagnosis of the disease. MRI has become increasingly popular among radiographic techniques due to its non-invasive nature and enhanced imaging capabilities compared to CT. Nevertheless, manual MRI scan analysis remains a challenge since it is a time-consuming and labour-intensive process. Additionally, medical experts must examine each scan slice by slice painstakingly.

## 1.2 Motivation

The advancement of Machine Learning and Deep Learning technologies, notably Convolutional Neural Networks (CNNs), offers powerful means for automatic feature extraction from image data and supporting medical professionals in diagnostic tasks. One crucial aspect of Crohn’s Disease diagnosis is the examination of the terminal ileum (T.I.). Holland et al.’s study [8] in 2019 proposed a residual network specifically targeting the terminal ileum to facilitate automated detection of Crohn’s Disease using MRI scans. The authors claimed that the efficacy of their framework was contingent upon the degree of localisation during the preprocessing stage. Consequently, they advocated for incorporating terminal ileal ground-truth segmentations to enhance the localisation of the terminal ileum and improve the performance of automated detection techniques.

In a subsequent study, Abidi et al. [9] advanced this line of research by developing an innovative deep-learning segmentation based on semi-supervised learning techniques and the nnU-Net architecture [10]. This approach utilised the centerline coordinates of the critical region to augment the data during training time, thus enabling the automatic localisation of critical regions. Abidi et al.’s research mainly focus on the localisation terminal ileum, which is essential for radiologists during diagnostic assessments. The researchers addressed the previously identified limitations regarding the high dependence on localisation during the preprocessing phase [8]. Furthermore, their findings established a solid foundation for a multi-class terminal ileum segmentation algorithm that combines transfer learning strategies with the nnU-Net architecture.

Inspired by the insights from [8, 9], this project aims to continue the work performed by [9], leveraging advanced deep-learning techniques to enhance the segmentation performance of the terminal ileum in MRI scans. The

successful accomplishment of this objective will significantly aid clinicians in diagnosing Crohn’s disease, ultimately contributing to enhanced patient outcomes.

### 1.3 Machine Learning Challenges

The efficacy of deep learning models is intrinsically linked to the training data’s quality, quantity, and diversity. One of the principal challenges faced in this project is the limited availability of training data. The dataset at our disposal is relatively small, comprising only 233 patient cases for three modalities of MRI scans, which pales compared to those utilised in other industry-leading deep learning systems.

Our image data’s region of interest (ROI) occupies a minor portion of the MRI scan. Additional preprocessing techniques, such as bounding box localisation and cropping, must be considered for enhancing the segmentation model’s performance, as suggested by [9]. Another major challenge is the necessity for manual segmentation by clinical experts to develop gold-standard labels or point-wise centerlines for patient data. This is indeed a complex, laborious, and inefficient endeavour. Consequently, acquiring high-quality and abundant patient data and gold-standard annotations poses significant challenges.

To mitigate these concerns, we propose a proxy training task employing weak supervision to generate coarse-grained segmentation masks as a compromise for the scarcity of gold-standard segmentations. Upon completion of the proxy task, gold-standard segmentations will be integrated into the training process to produce the final segmentation model. Prior also research [9] indicates that implementing transfer learning for proxy training [11] or incorporating a related pre-training job may serve as potential solutions to address these limitations.

### 1.4 Objectives

This project uses deep learning methodologies to construct an enhanced terminal ileum segmentation model based on prior work. To achieve this, we will solidify the previous research as a firm foundation and then incorporate sophisticated transfer and semi-supervised learning techniques. The specific objectives that inform our strategic approach include:

- We aim to establish a nnU-Net-based baseline segmentation model from the based prior work. The model training includes a proxy task and a fine-tuning task. In the proxy task, we propose generating coarse-grained weak masks with centerline coordinates of the critical region

with Simple Linear Iterative Clustering (SLIC) method for data without ground-truth annotations. These masks serve as a foundation for establishing the proxy training task. After training the proxy model using the generated weak masks, we plan to use the proxy model in conjunction with fully annotated data to develop our target segmentation model. This target model will set the baseline for subsequent refinement.

- Once our baseline is set, we plan to have another approach to generate weak masks in the proxy task by utilising the pre-trained SegmentAnything Model [12] from Meta AI. We will work on its medical imaging variant, MedSAM and fine-tune the model with our dataset. After fine-tuning, we can use the MedSAM model to generate weak masks, using the weak masks to complete the proxy task and obtain a refined model with full supervision.
- An essential part of our project is monitoring and quantitatively evaluating the performance of all developed models. We will compare the Dice Similarity Coefficient (DSC) to assess the quality of generated weak masks and the final segmentation performance between the baseline and our refined model. Additional statistical tests, such as t-test or f-test, will be applied to validate the statistical significance of our model's performance. To investigate the effect of possible critical components for the model training, ablation studies will be performed to analyse the importance of elements in the training trajectory.

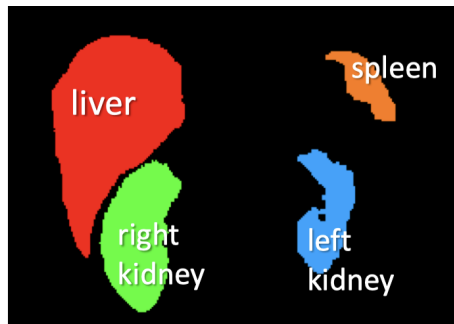
# Chapter 2

## Background

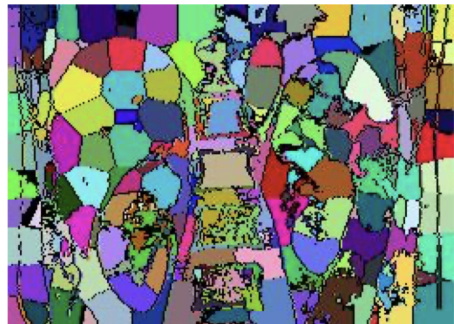
### 2.1 Delving into Image Segmentation

Image Segmentation is a fundamental concept in computer vision, demonstrating how machines perceive and understand image data. The topic of **semantic segmentation** is the essential part of this area. Semantic segmentation transcends the act of partitioning an image into various regions. It assigns each segmented region with a label, i.e. a **semantic meaning**, indicating what the region denotes. An illustrative example is provided in [Figure 2.1a](#), where the red region denotes the liver in a medical imaging scan.

One worth mentioning is that semantic segmentation distinguishes itself from other tasks that merely cluster images into coherent regions, as shown in [Figure 2.1](#) [13]. The regions identified through semantic segmentation carry a specific value or meaning inherently linked to the task at hand. In short, not just ‘where’ but ‘what’ is just as crucial in semantic segmentation.



(a) Semantic Segmentation



(b) Segmentation based on clustering

Figure 2.1: Different Image Segmentation Tasks

Having laid out an overview of semantic segmentation, we will delve deeper into the distinctive methodologies utilised for segmentation tasks in the following sections. This preliminary understanding provides a critical

foundation for exploring more complex segmentation strategies and their applications in tasks such as diagnosing diseases or enhancing medical imaging methods.

## 2.2 Manual Segmentation

Manual Segmentation, while basic, forms a cornerstone in image segmentation. In the context of our project, it involves utilising the specialised knowledge of medical experts to create ‘gold standard’ labels for MRI data. This process requires careful slice-by-slice examination of the MRI data, highlighting the region of target organs or the diseased from the healthy tissues. This level of detailed inspection ensures that such manual segmentation results in validated and trustworthy classifications.

However, manual segmentation does bring to light significant challenges. Notably, the time-intensive nature of this process becomes increasingly essential when dealing with large datasets. This situation is further compounded in scenarios requiring slice-by-slice analysis of MRI data. The result is that manual segmentation can be exceptionally time-consuming, limiting the volume of data labelled within an acceptable timeframe.

This leads us to confront an ever-present challenge: the scarcity of gold standard labelled data. The considerable investment of time and skilled resources required for manual segmentation naturally restricts the availability of such high-quality, expert-classified data sets. As we journey towards leveraging machine learning methodologies in medical imaging, this scarcity of gold-standard, manually segmented data exerts a substantial hurdle to overcome. Thus, innovative solutions are required to address this gap and enhance the effectiveness and efficiency of image segmentation processes.

## 2.3 Region-based Methods

Region-based segmentation techniques, with the region-growing method as a prominent example, offer an alternative approach to image segmentation. This method hinges on the premise of homogeneity within the segmented regions. The algorithm initiates with a seed pixel and then expands the region by successively incorporating pixels similar to the initial seed. The process continues until the region growth reaches a pre-defined size or once the region achieves homogeneity, which is interpreted as the point when neighbouring pixels become significantly dissimilar [14].

The region growth method often proves effective because it generates a connected region starting from the seed point. Unlike thresholding methods that rely on explicit image properties, region-growing methods facilitate segmentation based on pixel similarity. However, this method exhibits sensitivity to noise, as the algorithm may persist in growing the region even if

the neighbouring pixels significantly deviate from the seed pixel's properties.

Another key challenge when employing the region-growing method is the critical significance of the initial seed point selection. An incorrect choice of the seed point could obstruct proper region growth. This initial phase often becomes time-consuming and lacks accuracy when seeking the optimal seed point. Furthermore, it necessitates human intervention to evaluate the appropriateness of the chosen seed point.

## 2.4 Deep Learning Methods

### 2.4.1 U-Net: An Automated Deep Learning Method for Image Segmentation

U-Net [15] represents a transformative approach in the realm of deep learning methodologies for image segmentation. U-Net integrates a high-level contextual extraction path with a symmetric localisation pathway as an evolved variant of Fully Convolutional Networks (FCN) [16]. This unique arrangement captures a broad context of the image and enables precise localisation of the targets. This is ideal for creating an automated pipeline for T.I. segmentations and an essential requirement in our research.

The end-to-end learning facilitated by U-Net directly generates pixel-wise segmentation masks from raw pixels, creating a valuable asset for our project. The architecture of this robust network is illustrated in [Figure 2.2](#).

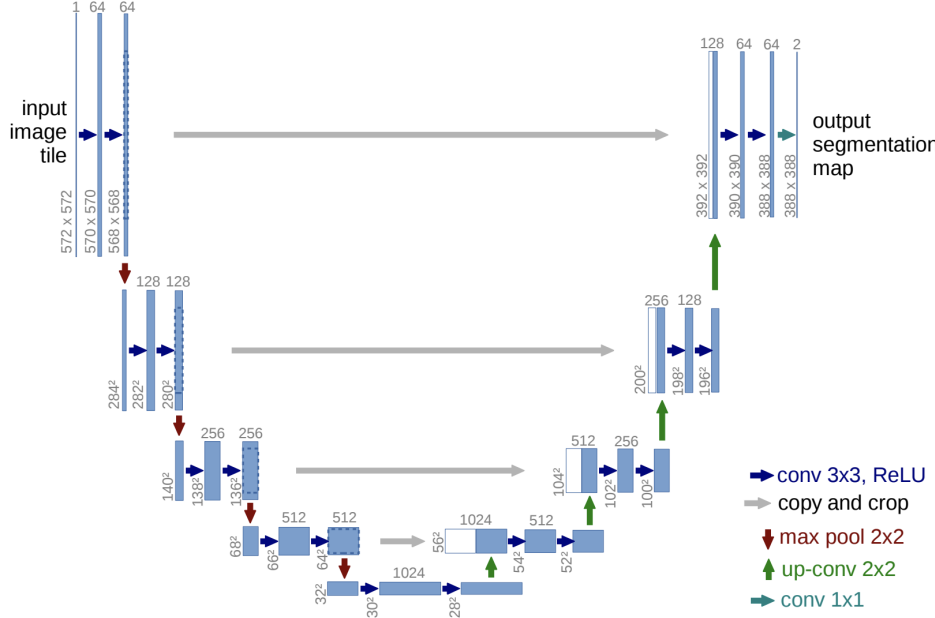


[Figure 2.2](#): An example of the U-net architecture.

U-net has also been developed to handle 3D data, which aligns perfectly with our scenario, where the MRI scans are inherently 3-dimensional images. Furthermore, each blue box in [Figure 2.2](#) encapsulates a multi-channel feature map. The number of channels is denoted at the top of each box, while the  $x$ - $y$  dimensions are annotated at the lower left corner of the box. Meanwhile, the white boxes signify sets of copied feature maps, with arrows demonstrating various operations.

The design on the network’s contracting (left) side entails a series of recurrent steps. Each step initiates with two 3x3 convolutions, proceeding to double the number of feature maps. The result is then subjected to a Rectified Linear Unit (ReLU) activation function, followed by a downsampling operation using 2x2 max pooling with a stride of 2.

The process commences on the network’s expansive side (right) with an upsampling step. A 2x2 convolution follows, halving the feature channels concatenated with their corresponding features from the contracting pathway. To conclude, a pair of 3x3 convolutions are applied to the image, succeeded by ReLU activations. The final layer employs a 1x1 convolution that maps each 64-component feature vector to the desired classes.

Overall, U-Net offers a comprehensive and highly effective tool for achieving granular image segmentation, which is indeed a capability integral to the success of our research exploration.

#### 2.4.2 nnU-Net: A Self-configuring Framework Aligned with Our Research Goals

The nnU-Net [\[10\]](#) offers a progressive step towards personalised segmentation techniques. As a framework built upon U-Nets, it embodies a self-configuring segmentation mechanism, which autonomously orchestrates the configuration of preprocessing, network architecture, training, and post-processing steps in a segmentation pipeline. Crucially, the configuration selected is not static but instead adapts to the specificities of the medical data used for training.

A standout feature of nnU-Net is its unique approach towards determining hyperparameters. The framework utilises “data fingerprints” allied with heuristic rules to pinpoint the optimal hyperparameter configuration for a given dataset before processing the training data. This data fingerprint concept is further leveraged to generate pipeline configurations, encapsulating inferred parameters (such as image resampling, normalisation, batch, and patch size) and blueprint parameters (such as loss function, optimiser, and network architecture).

With these pre-selected hyperparameters and generated pipeline configurations, nnU-Net proceeds to facilitate network training for 2D, 3D full-resolution, and 3D-Cascade U-Nets [\[17\]](#). The platform then selects an ensemble of configurations from these three networks to achieve optimal per-

formance (for instance, maximising the average dice coefficient). Once identified, this optimal configuration is subsequently deployed and evaluated on the test dataset.

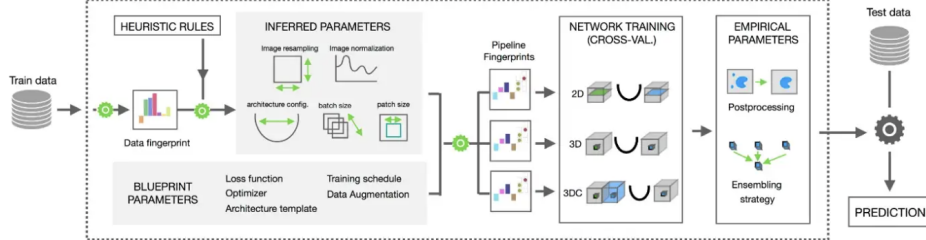


Figure 2.3: The pipeline representation of nnU-Net.

Notably, nnU-Net has been shown to deliver state-of-the-art performance in various medical imaging tasks, including segmenting brain tumours, prostate tissues, and liver structures [18].

Therefore, while nnU-Net enables a highly adaptive and automated segmentation workflow, the utility of the trained model is maximised when deployed on tasks that closely resemble the context and content of the training data. In our specific case, we will train the nnU-Net model with our particular type of 3D MRI scans for T.I. segmentation tasks to ensure optimal results. This approach ensures leveraging the full potential of nnU-Net's adaptive capabilities tailored to our research goals.

As our research strives to establish an automated pipeline for T.I. segmentations on 3D MRI scans, integrating the nnU-Net framework is poignantly relevant. With its inherent capacity to adapt to different datasets and consistently yield precise image segmentation, nnU-Net is excellently positioned to enhance the rigour and precision of our research endeavour.

## 2.5 Generating Weak Labels: A Strategic Response to Annotation Scarcity

Given the scarcity of gold standard annotations for segmentation tasks, as discussed in section 2.2, it becomes imperative to identify effective strategies that can enhance our training outcomes. One potential approach is using weak labels or weakly-segmented masks derived from the data. By adopting such methods, we aim to extract critical image features that can contribute to the learning efficacy of our model, despite limited access to manually-annotated, gold-standard data.

### 2.5.1 Leveraging Unsupervised Methods: Simple Linear Iterative Clustering (SLIC)

Simple Linear Iterative Clustering (SLIC) [19] is a unique unsupervised method we contemplate employing. This algorithm stands at the forefront of superpixel segmentation techniques, providing a powerful tool to cluster pixels within an image into compact and uniformly labelled regions, referred to as ‘superpixels’.

The key strengths of SLIC are its simplicity, ease of implementation, and adaptability across diverse scenarios. These virtues enable SLIC to handle boundary adherence issues effectively while reducing the computational burden associated with image segmentation tasks. SLIC operates as a spatially constrained iterative k-means clustering method with a pre-determined superpixel. [Figure 2.4](#) illustrates the effect using SLIC.

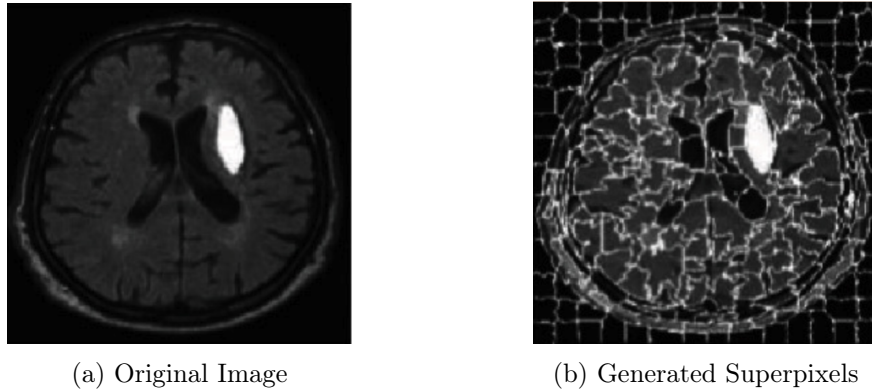


Figure 2.4: Superpixel Segmentation using SLIC

---

#### Algorithm 1 SLIC superpixel segmentation

---

- 1: Initialise cluster centers  $C_k = [l_k, a_k, b_k, x_k, y_k]^\top$  by sampling pixels at regular grid with grid interval  $S$ .
  - 2: Perturb cluster centers in a  $n \times n$  neighbourhood, to the lowest gradient position.
  - 3: **while**  $E >$  threshold **do**
  - 4:     **for** each cluster center  $C_k$  **do**
  - 5:         Assign the best matching pixels from a  $2S \times 2S$  square neighbourhood around the cluster according to the distance measure [19].
  - 6:     **end for**
  - 7:     Compute new cluster centres and residual error  $E$ .
  - 8: **end while**
  - 9: Enforce Connectivity.
-

The SLIC algorithm adapted from [19] is illustrated in [Algorithm 1](#). Additionally, the residual error  $E$  in clustering is defined as the  $L_1$  distance between previous centres and recomputed centres.

By integrating SLIC as part of our weak label generation strategy, we aim to utilise these inherent benefits to enhance the robustness of our machine learning models, thereby bringing rich insights from our medical imaging data in the absence of extensive manually-curated annotations.

### 2.5.2 Harnessing Pretrained Models: The Segment Anything Model (SAM)

Emerging from the innovative approaches of Meta AI, the Segment Anything (SA) project presents a new paradigm for image segmentation. The cornerstone of this project is a pioneering model known as SAM, which exhibits an impressive degree of adaptability and transferability. Specifically designed and trained to be promptable, SAM showcases remarkable capabilities in zero-shot transfer to new image distributions and tasks.

This inherent agility of SAM incites impressive zero-shot performance outcomes. Indeed, comparative analysis with prior fully supervised results reveals that SAM often delivers competitive, even superior, performance metrics [12]. Extending this versatile approach to medical imaging, MedSAM [20] offers compelling prospects. Derived from the parent SAM model, MedSAM has shown considerable promise in segmenting medical images. One study unearthed that SAM’s functionality can be enhanced with manual prompts, such as points and boxes, indicating intended objects in medical images [21]. This enhancement strategy aligns perfectly with our proposed approach to utilise the centerline coordinates and refine the segmentation process by obtaining finer-grained weak masks from SAM and MedSAM.

With its inspiring capabilities, the SAM model family holds immense potential to enhance our quest for automated and precision-driven segmentation techniques, thereby bolstering our research outcomes.

# Chapter 3

## Related Work

### 3.1 Automatic Detection and Segmentation of Crohn’s Disease Tissues from Abdominal MRI

The origins of applying deep learning techniques to medical image analysis can be traced back to approximately a decade ago. In 2013, Mahapara et al. [22] pioneered a machine learning-based method for segmenting bowel regions to detect Crohn’s disease tissues in MRI scans.

The proposed pipeline begins with over-segmenting the input MR image test volume into supervoxels. Random Forest (RF) classifiers identify supervoxels containing diseased tissues, subsequently defining the Volume of Interest (VOI). Within the VOI, voxels are further examined to segment the affected region. An additional set of RF classifiers is applied to the test volume to generate a probability map, delineating the likelihood of each voxel being classified as diseased tissue, normal tissue, or background.

Empirical results demonstrate that this approach achieved satisfactory segmentation performance, evidenced by a Dice metric value of  $0.90 \pm 0.04$  and a Hausdorff distance of  $7.3 \pm 0.8$  mm. The significance of this research lies in developing an automated pipeline for segmenting diseased bowel sections in abdominal MR images. This pipeline assists medical experts in identifying affected tissues, thereby facilitating the diagnosis and treatment of Crohn’s Disease. The clinical validation of the results, showcasing high segmentation accuracy, further underscores its utility in supporting medical professionals in their work.

Nevertheless, the method is limited by computational inefficiency and complexity due to extended testing times for each instance, fine-tuning requirements for each pipeline stage, and ample opportunities for architectural improvements. Moreover, the research does not delve into finer details, such as the terminal ileum, which is crucial for comprehensive analysis and early diagnosis.

## 3.2 Automatic Detection of Bowel Disease with Residual Networks

Building on several years of research in the field, Holland et al. [8] put forth a pioneering approach in 2019 to automate the detection of Crohn’s disease from a limited dataset of MRI scans. The authors employed an end-to-end residual network [23], equipped by a soft attention layer [24]. This layer essentially magnified salient local features and added a layer of interpretability, providing a clearer understanding of the analytical process.

Their approach exclusively targets the terminal ileum in a strategic departure from semantic segmentation strategies typically employed. This focus underscored the potential feasibility of deep learning algorithms for precisely identifying terminal ileum Crohn’s Disease within abdominal MRI scans.

The method’s robustness is reflected in its experimental results. Under conditions of localised data within a semi-automatic setting, the model achieved a commendable weighted-f1 score of 0.83. This score is particularly noteworthy given its close correlation with the MaRIA [25] score, a clinical standard that enjoys widespread acceptance in the medical community. Beyond its performance metrics, the researchers accentuated the relative efficiency of their model, which necessitated only a fraction of the preparation and inference time compared to standard procedures. This aspect underlines the potential for significant time-saving benefits in a clinical context.

However, the research did reveal certain limitations. Notably, when applied in a fully automatic setting, the model’s performance exhibited a marginal decrease in efficiency. Although this does not detract from the study’s overall achievements, it highlights an area where further refinement and improvement could be pursued.

Reiterating their discoveries, Holland et al. proposed a strong correlation between model performance and the degree of localisation in the training data. They suggested the collection of gold-standard segmentation of the terminal ileum could prove beneficial as an antecedent task in enhancing automatic detection performance. This proposition opens up intriguing possibilities for research, including the work presented in this thesis, which explores these aspects in greater detail.

Their insights illuminate the synergistic potential between manual analysis and automated methods in enhancing diagnostic capabilities. Importantly, they establish a pathway for integrating deep learning techniques to detect Crohn’s disease from limited datasets, indicating a promising approach to tackle one of the significant challenges in machine learning: data scarcity. By leveraging soft attention mechanisms to intensify salient local features and augment interpretability, they provide a valuable tool for medical professionals to comprehend better the results generated by the al-

gorithm.

These findings, particularly the proposed use of gold-standard segmentation of the terminal ileum, provide a solid foundation for the work pursued in this thesis.

### 3.3 Leveraging Machine Learning Methods for Accurate Prediction of Intestinal Damage in Crohn’s Disease Patients

In 2020, Enchakalody et al. [26] embarked on an innovative study exploring the potential of machine learning methodologies to enhance the precision and reliability of diagnosing and monitoring Crohn’s Disease. They applied these techniques to a small dataset of 207 CT-Enterography (CTE) scans, an approach that mirrors our research focus. Their comprehensive analysis involved examining cross-sectional views of small intestine segments and precisely detecting diseased tissues. Utilising two distinct classifier types - Random Forest (RF) with ensemble techniques and Convolutional Neural Network (CNN) algorithms, they quantitatively evaluated intestinal damage related to Crohn’s Disease on each mini-segments.

The efficacy of both RF and CNN techniques was compellingly demonstrated in the experimental results, achieving accuracy rates of 96.3% and 90.7%, respectively, for classifying diseased and normal segments. Remarkably, these techniques mirrored the effectiveness of expert radiologists in distinguishing between diseased and normal small bowel tissue. This underscores the immense potential of machine learning, even when applied to small datasets, in elevating the precision of Crohn’s Disease diagnoses.

The research conducted by Enchakalody et al. is particularly insightful for our work. It demonstrates the successful application of deep learning techniques on small datasets and opens the door to potentially revolutionising the diagnosis and treatment of Crohn’s disease through machine learning. It highlights the possibility of a more precise and automated approach to detecting intestinal damage in such patients, a focus that aligns closely with our current research aims.

While it should be noted that this study primarily focused on data derived from CT-Enterography, differing slightly from our focus on MRI data, the methodology and findings offer valuable insights. As of the time of writing this report, despite the progress made, achieving a fully automatic approach for diagnosing Crohn’s disease based on cross-sectional imaging that equates to the proficiency of expert radiologists continues to be an exciting area of ongoing research.

## Chapter 4

# Ethical Discussion

Given the sensitive nature of our project that involves the handling of medical data, we are steadfastly committed to ensuring a robust ethical framework guide all phases of our work. This initiative encompasses further processing and augmentation of previously collected medical data and merging existing datasets.

To safeguard personal identity and ensure strict adherence to privacy standards, all MRI scans are carefully processed under the oversight of clinical radiologists at St Mark Hospital. Comprehensive measures remove any personally identifiable data from the medical records, such as names, genders, ages, and ID numbers. As a result, it is impossible to trace any individual's identity from the processed medical data.

Our commitment to ethical considerations extends into the model training procedure. We employ the nnU-Net framework, which utilises convolutional layers to learn from data via feature extraction. This learning procedure does not store original training data; instead, it creates feature maps representing distilled, valuable insights from the data. This process ensures that the original training data cannot be recovered from the model, thereby preserving individual privacy.

Our project is on a foundational ethical commitment that respects personal anonymity and data confidentiality. Recognising the crucial importance of trust in scientific inquiry, mainly when dealing with sensitive medical data, we are dedicated to exemplifying conscientious practices that uphold the highest standards of research ethics.

# Chapter 5

## Dataset Analysis

In this chapter, we will delve into the composition of our dataset and perform an exploratory analysis of the dataset.

### 5.1 Dataset Exploration

Our research utilises T2-weighted MRI images to help with segmentation tasks. T2-weighted images are a specific genre of MRI scans manifested by the heightened intensity in fluid-rich structures, while their fat-laden counterparts appear darker.

In enriching the diversity of our dataset, we have judiciously incorporated three variants of MR images. Each image class contains 233 MR scans obtained by St. Mark's Hospital radiologists.

A summary describing each variant's unique features and applications is as follows, and the difference between images can be further visualised in [Figure 5.1](#) below.

- **Axial T2-weighted Images:** Projected along the axial plane, these images provide a top-down representation of anatomical structures and are especially beneficial in examining anatomical correlations.
- **Coronal T2-weighted Images:** Imaged along the coronal plane, these scans offer a frontal anatomy perspective. These images are reputable for their proficient highlighting of fluid-filled structures and lesions.
- **Post-Contrast Axial T2 Images:** These images are captured after administering a contrast agent and enhance tissue contrast, thereby providing enriched insights into the nature of lesions.

The strategic incorporation of three distinct forms of MR images enriches our dataset, transforming it into a comprehensive repository designed to

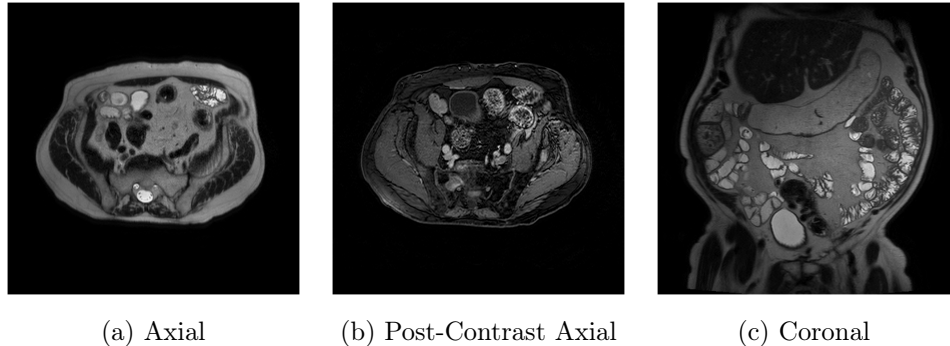


Figure 5.1: T2-Weighted MRI with different modalities in the dataset

master the intricate segmentation task. However, it is still apparent see potential obstacles such as MRI artefacts originating from patient movement or the overarching issue of data scarcity posing challenges to the success of the segmentation task.

The limited availability of annotated data affects the trajectory of the model training. It curtails our ability to effectively evaluate the model performance due to the restricted availability of testing data.

However, this scarcity of data fuels our quest for alternative annotated datasets to augment model training. The following chapter provides a detailed discussion of our innovative approach to addressing this challenge.

## 5.2 Dataset Specification

To have a detailed peek at the composition of our dataset, for each type of image, our dataset includes 113 abnormal cases and 120 normal cases in terms of diseased tissue in the abdominal scan. In addition to images, we also have a collection of centerline coordinates representing the colon in the MR image, although these are not available for every image. Furthermore, a select set of human-annotated ground truth results is included.

The generation of colon centerline coordinates is a meticulous process performed by radiologists via manual slice-by-slice inspection. After careful examination, they annotate the relevant slices with reference points linked to the colon. These annotations are archived as compressed XML files, colloquially referred to as **traces files**.

This storage format serves a dual purpose. Firstly, it facilitates visual inspection and analysis within the framework of medical imaging by clinical experts. Secondly, it empowers developers to navigate the XML tree to gather valuable information about the centerline coordinates. Notably, the preliminary 20% of the points are often deemed the most accurate, typically representing the interval in which the terminal ileum is situated.

Upon closer examination, the centerline and ground truth annotation distribution is shown in [Table 5.1](#). Note that there is no centerline provided for the post-contrast MRIs. Therefore the image data cannot be augmented via additional information such as centerline coordinates or bounding boxes. This will lead to difficulty obtaining a model with precise segmentation results on post-contrast MRIs, and we opt to focus on the **Axial and Coronal T2 MRI** only for further investigations.

Modality	Total Centerlines	Centerlines (abnormal:normal)	Ground Truth (abnormal:normal)
Axial	103	59:44	18:20
Coronal	93	46:47	18:30
Post-Contrast	-	-	13:20

Table 5.1: Distribution of centerlines and ground truth segmentations for different MR images

Our diverse and comprehensive dataset provides thoughtful insights for analysis and a solid foundation for reliable model training.

### 5.3 Ground Truth Segmentations

The ground truth segmentations delivered by our panel of clinical experts are assigned with varying semantic meanings, each corresponding to unique label IDs. The specifics of these relationships are highlighted in [Table 5.2a](#). I drew ten samples from each labelled image data to gain a clear segmentation overview and investigated the label distribution. It is thereby graphically demonstrated in [Figure 5.2b](#) represented on a logarithmic scale.

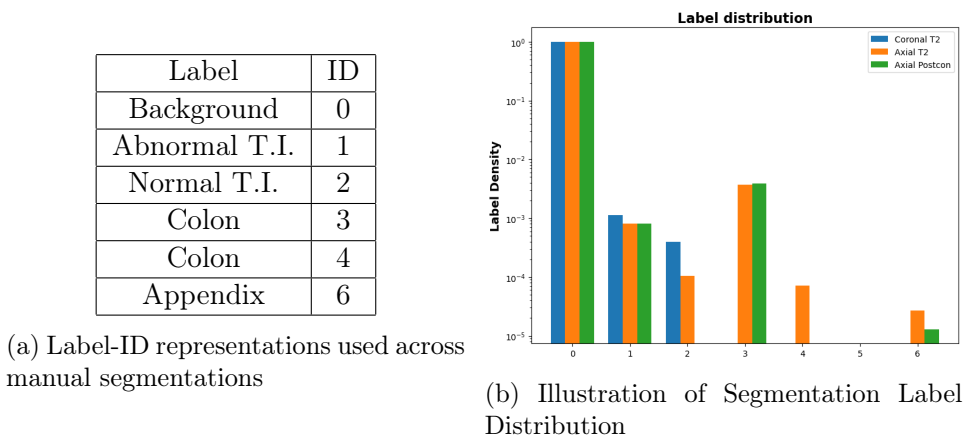


Figure 5.2: Detailed breakdown of segmentation specifics and label distribution across diverse categories of image data

From the results, a salient observation is the predominance of the background label in the voxel classes of the ground truth segmentation results. Its pronounced presence approximates one, rendering other voxel labels relatively insignificant and emphasizing the challenges intrinsic to abdominal MRI segmentation.

This raised a need for us to rethink the segmentation scope. Given the relative insignificance of portions other than the background, the informational value they contribute toward the training process is marginal at best. This little contribution not only impedes the ability of the model to classify effectively within these regions but increases the risk of false-positive classifications considering the comparison between the remaining regions versus the background.

To alleviate this issue, we simplify the scenario into a binary classification problem, interpreting all non-background voxels as general T.I. regions. Accurate segmentation of this region holds significant implications for enabling clinical experts to diagnose Crohn’s disease early.

This insight has inspired us to consider utilizing the centerline coordinates as a guiding factor for future initiatives. Specifically, we are contemplating two potential applications: augmenting the data through bounding box applications or minimizing the search space by cropping the image. This could balance the label distribution between background and T.I. regions, thereby improving the suitability of the segmented images for subsequent analyses. Ultimately, these initiatives aim to overcome the challenges identified in our exploration of ground truth segmentations.

# Chapter 6

## Methodology

The methodology is essential for the success of our segmentation task. In this chapter, we will discuss the key components of our methodology, including dataset preprocessing, baseline implementation, weak label generation, choice of the training settings, training pipeline and model inference. As the MRI data with different modalities presents varying features during model training, our methodology will be applied separately to both Axial and Coronal MRI and further investigate the cross-modality segmentation results.

### 6.1 Dataset Preprocessing

Our preliminary data analysis unveiled that non-background voxels comprise only a small fraction of the total MRI volume. As a result, they may not provide substantial information to facilitate effective learning for the segmentation model. To address this limitation, we harness the provided centreline coordinates of the terminal ileum to define a bounding box encompassing the T.I. region. Subsequently, the bounding box information will be encoded to prompts for refining the weak label generation with MedSAM. Details for this step will be covered in the model training part later.

Furthermore, we employ traditional image processing methods to streamline the data further. These include resizing and image normalisation, which abate the complexity of the data while maintaining consistency within the dataset.

Before commencing training, we must format the dataset following nnU-Net’s requirements [10]. After a successful conversion, nnU-Net undertakes to preprocess by adjusting images to various dimensions and resolutions and optimising them for ensemble model training. Simultaneously, it generates a unique ‘**dataset fingerprint**’, which proves invaluable during subsequent hyperparameter tuning. With these prerequisites satisfied, the preprocessed dataset stands ready for proxy learning.

This rigorous and systematic approach to data preprocessing ensures our

model is equipped with well-structured data, which is critical in enhancing its learning efficiency. Consequently, this results in improved accuracy of the generated segmentations, thus underlining the importance of adequate dataset preprocessing in clinical imaging analysis.

## 6.2 Baseline Implementation

Building upon precedent research, we've formulated a baseline model that adheres to a systematic and robust methodology. This model lays the groundwork for further enhancement and modifications later in our project:

Our first step involves the application of 3D Simple Linear Iterative Clustering (SLIC) superpixel segmentation on the cropped Region of Interest (ROI), where the ROI is defined through centerline coordinates. This task generates a weak mask that becomes instrumental in our proxy learning stage. To ensure the successful execution of this step, we identify the superpixels situated on the centreline of the terminal ileum, leveraging provided centreline coordinates. Subsequently, the segmented superpixels are relabelled to binary labels, as it realigns output with our project objectives.

Upon generation of the initial segmentation, we confront the potential issue of a hole or tube-like structures within the segmented supervoxels. These irregularities can disrupt the continuity of the terminal ileum representation. Therefore, our process incorporates a voting iterative binary hole-filling algorithm and morphological hole-closing to create a more refined segmentation.

With the generation of weak masks accomplished, we train our proxy model. Furthermore, a second training iteration is conducted, deploying the proxy model on fully-annotated data to obtain the final segmentation model. The following sections will discuss additional aspects of the training process and the ensembling strategy employed to derive the final model.

## 6.3 Model Training

As we step into our process, our attention is directed towards the pivotal stage of model training. This stage is characterised by an enriched proxy learning strategy, where we replace the initial unsupervised 3D SLIC-based weak mask generation with a more sophisticated tool: MedSAM. The training and evaluation phases are also designed to optimise model performance, incorporating cross-validation and ensemble learning methods. Below, we elaborate on these critical aspects:

- **MedSAM Application:** In this subsection, we discuss in detail how we leverage MedSAM for generating high-quality weak masks, adapting our MRI dataset to MedSAM via fine-tuning and elucidating its superior capabilities in medical image segmentation and its specific role in enhancing our model learning trajectory.

- **Dataset Partitioning:** Here, we explain how we divide our dataset into training and testing sets using an 80/20 ratio. We provide a rationale for this split and discuss how it ensures a robust and unbiased evaluation of our model performance.
- **Training Pipeline:** Our multifaceted training pipeline starts with a two-phased approach. Initially, we train a proxy model on weak masks generated by MedSAM. This is followed by further training on 80% of the fully annotated data, maximizing learning from weak and fully annotated data sets.

To ensure model robustness, a 5-fold cross-validation method is integrated during training to mitigate overfitting risks. Furthermore, our pipeline supports different configurations, which include 2D and 3D variants of data, loss function adjustments, and variations in training optimisers and learning rates.

The final aspect of our pipeline is ensemble learning, utilized to aggregate models across different folds and configurations, thereby generating our target model. The collective operation of these facets is meticulously designed to bolster our model performance in diverse scenarios.

- **Inference:** In this final stage, we delve into utilising the trained model for making inferences. We outline the procedural aspects of applying the model to new and unseen data, thus generating predictive outcomes that form the basis for the subsequent comprehensive evaluation of our model performance. The evaluation process, with detailed quantitative analysis, will be discussed extensively in the following chapter.

Through this comprehensively planned model training phase, we aim to build a proficient terminal ileum segmentation model that learns effectively from our data and showcases robust performance across varying scenarios.

### 6.3.1 Refining Weak Masks with MedSAM

The enhancement of our weak masks is a crucial cornerstone of our strategy. To achieve this, we utilize MedSAM - a modified version of the SegmentAnything Model specifically designed for medical images. Its bespoke design facilitates the creation of finely-tuned and detailed weak masks, setting a solid foundation for superior segmentation outcomes.

Our journey begins by introducing our preprocessed images to the MedSAM model. Traditional methodologies often fall short when compared with this advanced tool. MedSAM's core strength lies in its innovative AI algorithms identifying unique attributes embedded within medical images. This capability enables the production of granular segmentations far surpassing

the precision attainable through conventional models. A fine-tuning process is executed to reconfigure the MedSAM model for compatibility with our dataset and ensure the generation of high-quality, refined masks. This involves training the pre-trained MedSAM model on fully annotated ground truth segmentations.

Once the fine-tuning phase wraps up, we leverage SAM to generate weak masks on images devoid of full annotations. An integral part of our weak label generation includes bounding boxes focusing on the T.I. region, as defined by centerline coordinates. As substantiated by Huang et al., 2023 [21], such augmentation amplifies the quality of the resulting weak mask. For those images that lack provided centerline data, we opt to exclude them from our dataset. This ensures a coherent and reliable pool of data driving our methodology forward.

Incorporating MedSAM into our workflow signifies a pivotal stride towards achieving phenomenal segmentation outcomes. The emergence of refined masks unveils new dimensions of learning for our model, cementing a robust foundation for subsequent breakthroughs in terminal ileum segmentation.

### 6.3.2 Executing Dataset Partitioning

Partitioning our dataset into training and testing sets is crucial in our model development. This strategy helps assess the model performance on new, unseen data, establishing a reliable measure of its predictive capabilities.

Our approach involves a partitioning of the dataset into an 80/20 ratio. Before this division, we shuffle the dataset to randomise the order of samples, ensuring an unbiased representation in both the training and testing sets. Subsequently, the first 80% of these randomized samples form our training set, while the remaining 20% are reserved for testing.

The reason for using such a ratio is that it is widely revered in machine learning and serves to strike a balance between providing sufficient data to nourish the model’s learning journey and withholding a substantial portion for an authentic evaluation of its performance. This balance becomes particularly crucial when navigating through scenarios characterised by a limited dataset, such as ours.

This cautious allocation of data equips us with a model that’s not only well-trained but also rigorously tested for its predictive performance, strengthening our confidence in its segmentation ability.

### 6.3.3 Establishing the Training Pipeline

This subsection outlines on principal components of our training pipeline, including the deliberate choices and reasonings behind formulating the loss function, selecting the optimiser and determining the learning rate. A two-

phased training approach with the key components is proposed to ensure the model's capability to learn efficiently, navigate an optimised prediction path, and deliver robust T.I. segmentation.

### **Loss Function Formulation**

Guiding the learning trajectory of our model during training is an elegantly designed loss function. Particularly, we harness nnU-Net's unique blend of cross-entropy and Dice losses [27], expressed as:

$$\mathcal{L} = \mathcal{L}_{CE} + \mathcal{L}_{Dice}$$

For our specific use case, this composite loss function manifests into a binary form, simplifying to a binary cross-entropy loss defined as:

$$\mathcal{L}_{CE} = \sum_i^N (y_i \log o_i + (1 - y_i) \log(1 - o_i))$$

In this equation,  $y_i \in \{0, 1\}$  symbolizes the ground truth label for the  $i$ -th instance, while  $o_i \in [0, 1]$  represents the corresponding sigmoid probability for the given label  $y_i$ .

Complementing this, the Dice loss is articulated as:

$$\mathcal{L}_{Dice} = -\frac{2 \sum_i^N o_i y_i}{\sum_{i=1}^N (o_i + y_i)}$$

Here,  $N$  encapsulates the total number of pixels in the training batch.

Carefully orchestrating these two components within the loss function empowers our model to traverse the complex learning landscape effectively, optimising its performance in terminal ileum segmentation.

### **Optimiser Selection**

In constructing an effective training strategy for our model, we deploy Stochastic Gradient Descent (SGD) as the principal optimizer, supplemented by a Nesterov momentum set to 0.99.

This process can be imagined as an expert guide traversing complex terrain, searching for the lowest point or valley - an analogy for the optimal solution that minimizes error. In this context, SGD serves as our skilled explorer, persistently heading towards the steepest downward gradient in pursuit of the valley.

However, as any experienced guide attests, the steepest descent does not necessarily lead to the lowest valley due to potential undulations and terrain variations.

Addressing this challenge is the role of the Nesterov momentum. It equips our guide with a metaphorical telescope, allowing for a foresighted view of

the landscape along the current path before finalising the next step. This foresight permits more informed decisions considering the overall landscape rather than the immediate surroundings.

This stands in contrast to the classical momentum method, which can be considered a hiker relying solely on their current position and pace to determine their next step without any foresight or scouting tools. An intuitive illustration of the difference between the effect of classical and Nesterov Momentum is shown in [Figure 6.1](#) [28].

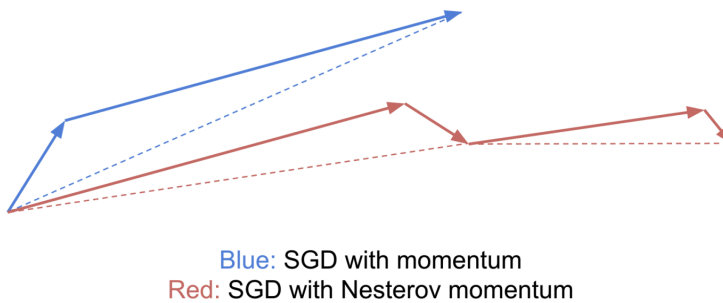


Figure 6.1: Nesterov momentum

Employing Nesterov momentum with our SGD optimizer enables a quicker and more precise journey to the ‘valley’ or optimal solution, ensuring our model learns effectively and efficiently from our data.

To illustrate this concept more clearly, [Algorithm 2](#) outlines this process in detail:

---

**Algorithm 2** SGD enhanced with Nesterov Momentum

---

**Require:** Initial learning rate  $\eta$ , momentum  $\beta$

**Require:** Initial parameter  $\theta_0$ , initial velocity vector  $v_0$

- 1: **while** not reaching stopping criteria **do**
- 2: Draw one batch with  $m$  samples  $x^{(1)}, \dots, x^{(m)}$  with corresponding  $y^{(i)}$
- 3: Temporarily update the parameter:  $\tilde{\theta}_t \leftarrow \theta_t - \beta v_t$
- 4: Compute the gradient at the adjusted point:

$$g_t \leftarrow \nabla_{\tilde{\theta}_t} \sum_i \mathcal{L}(f(x^{(i)}; \tilde{\theta}_t), y^{(i)})$$

- 5: Refresh the velocity:  $v_{t+1} \leftarrow \beta v_t + \eta g_t$
  - 6: Update the parameter:  $\theta_{t+1} \leftarrow \theta_t - v_{t+1}$
  - 7: **end while**
- 

In more technical terms, the Nesterov momentum method facilitates accelerated learning relative to traditional methods. This acceleration is of crucial strategic value, as it leads to significant time and resource efficiency.

cies, thereby boosting the progression of our model into a highly competent predictive tool in a shorter span.

### Learning Rate Determination

The learning rate is crucial in optimising our model, which guides the magnitude of updates made to learnable parameters during each iteration. We have set an initial learning rate of 0.01 to balance by ensuring that our model learns steadily without missing out or skipping over essential information.

However, the critical characteristic of our approach is that our learning rate is not constant — it gradually decreases as training progresses. This strategy, known as learning rate annealing or decay, is essential in optimising our model performance.

As the training advances, model parameters tend to converge towards an optimal solution. Here, making significant adjustments is not ideal because it might cause the parameters to oscillate around (or overshoot) the desired optimum. To address this issue, we decrease the learning rate across iterations, encouraging smaller steps when we are presumably closer to the optimum and enhancing the model performance over time.

We employ a learning rate scheduler that uses a polynomial function determined by the total number of training iterations. The decaying learning rate,  $\eta_t$ , is computed by:

$$\eta_t = \eta_0 \left(1 - \frac{t}{N}\right)^{0.9}$$

Here,  $\eta_0 = 0.01$  is the initial learning rate,  $t$  stands for the current iteration count, and  $N$  represents the total iterations.

By carefully managing the learning rate via this method, we ensure that our model can adapt effectively across training steps, continually refining its performance with each iteration.

### Two-phased training

Our training pipeline adopts a two-phased strategy, heavily leveraging the loss function, optimizer, and learning rate detailed prior.

In the first phase, the proxy model is trained using the generated weak mask over 200 epochs, reserving 20% of the training data for validation. This process utilises an SGD optimiser with Nesterov momentum and an initial learning rate of 0.01 with our proposed strategy of learning rate decay. After completing this preliminary phase, nnU-Net collates the validation results and combines them with pre-extracted dataset fingerprints to finalise the optimal hyperparameter combination for the proxy model.

The subsequent phase fine-tunes the proxy model on fully annotated images across 50 epochs. A 5-fold cross-validation along with the same optimisation settings as the previous phase ensures a compelling learning trajectory.

Notably, only 80% of the fully annotated data feeds into this stage, preserving 20% of the data and their corresponding ground truth segmentations for the ultimate evaluation.

This two-phase strategy remains adaptable to varied data configurations, accommodating differences in image dimensions and resolutions while seamlessly integrating with 2D and 3D full-resolution data. We ensure each model concludes its training and strategically combine predictions on unseen gold standard data to determine the final output.

The selection of the final model is guided by cross-validation performance. Depending on the outcomes, the final model could either be a single best-performing model or an ensemble of models trained across different folds. Our objective remains consistent throughout this meticulously planned two-phase training: To create a proficient model capable of delivering exceptional terminal ileum segmentation.

#### 6.3.4 Executing the Inference Process

Once the optimal model is determined, we can introduce unseen, pre-processed data into the nnU-Net framework. This enables us to generate straightforward predictions. However, it is important to highlight several points that characterise this predictive phase.

In alignment with nnU-Net’s patch-based training procedure, inference also adopts a patch-based methodology. Each image is divided into smaller sub-images or ‘patches’, and it is upon these patches that our model bases its predictions. Nevertheless, another worth-mentioning point is that the model precision tends to decrease towards the edge of these patches. Consequently, when generating predictions, the model attributes greater significance to the voxels near the patch’s centre than their edge-located counterparts. This strategy ensures a notably higher prediction quality upon aggregating the predictions across all patches.

Upon the completion of the model prediction, a common practice is to apply post-processing to the generated predictions. Post-processing is often employed based on connected components to enhance image segmentation, such as organs. This approach typically centres on disregarding smaller, potentially insignificant elements and emphasising the most expansive interconnected region to mitigate the probability of false positives.

Exemplifying this philosophy, nnU-Net systematically utilises the implications of omitting these smaller entities on the model performance, employing cross-validation results as a reference metric. Initially, each foreground class is treated as a singular entity. If the constraint to the most significant region increases the average foreground Dice coefficient without diminishing any class-specific coefficients, this method emerges as the preliminary post-processing step. After the outcome of this stage, nnU-Net determines whether the same way requires the application to individual classes.

This sophisticated, multi-faceted approach to inference empowers us to maximise the accuracy, reliability, and clinical relevance of our terminal ileum segmentation predictions.

# Chapter 7

## Evaluation

With the culmination of our model’s training and inference phases, we now focus on its assessment. The heart of this chapter is to critically evaluate our model performance and authenticate its effectiveness against preceding works. Chapter 6 thoroughly explained the foundations and implementation of our baseline model, leveraging the SLIC algorithm, centerline coordinates, and extracted ROI. Consequently, we will not further discuss the baseline construction here. Instead, this chapter will identify and deploy effective evaluation methodologies and metrics. This allows us for a rigorous assessment of our model performance and the validity of its results, helping us understand the strengths and limitations of our model and suggesting potential directions for future improvement.

### 7.1 Evaluation metric

#### 7.1.1 Dice Similarity Coefficient (DSC)

The Dice Similarity Coefficient (DSC), or the Sørensen-Dice coefficient, is a robust metric for quantifying overlap. This statistic facilitates understanding how closely the predicted segmentation aligns with the ground truth, which is pivotal in assessing image segmentation tasks.

Suppose we have two sets  $X$  and  $Y$  representing our ground truth and predicted segmentation, respectively. The DSC is defined as follows:

$$\text{DSC} = \frac{2|X \cap Y|}{|X| + |Y|}$$

This equation encapsulates the ratio of twice the intersection of  $X$  and  $Y$  to the total sizes of both sets. Nevertheless, if we expand on this definition, we can express the DSC in another form that highlights its relation to classification metrics. This can be done by abbreviating True Positive, False Positive,

and False Negative predictions as TP, FP, and FN, respectively:

$$\text{DSC} = \frac{2 \text{TP}}{2 \text{TP} + \text{FP} + \text{FN}} = F_1$$

In this context, TP represents an agreement between our prediction  $Y$  and the ground truth  $X$ , where both identify a positive label. FP and FN, however, correspond to discrepancies between  $Y$  and  $X$ , which correspond to the areas where the classifier and ground truth disagree. This representation underlines the intimate relationship between DSC and classification metrics, demonstrating the capacity of the former to inform us about the precision and recall of our model, where both consider the significance of True Positives and penalise any False Positive predictions. Thus its utility in image segmentation evaluation can be seen.

### 7.1.2 Jaccard Similarity Coefficient

The Jaccard Similarity Coefficient is a well-established metric often associated with the DSC due to its role in evaluating the similarity and diversity of two sets. It quantifies the proportion of shared elements between the sets relative to their combined unique features—essentially measuring the overlap against the total spread.

Let us again consider two sets  $X$  and  $Y$ , representing the ground truth and predicted segmentation masks, respectively. The Jaccard Coefficient is defined as:

$$\text{JSC} = \frac{|X \cap Y|}{|X \cup Y|} = \frac{\text{TP}}{\text{TP} + \text{FP} + \text{FN}}$$

Further exploration allows us to rewrite the Jaccard Coefficient in the form:

$$\begin{aligned} \text{JSC} &= \frac{|X \cap Y|}{|X| + |Y| - |X \cap Y|} \\ &= \frac{\frac{|X \cap Y|}{|X| + |Y|}}{1 - \frac{|X \cap Y|}{|X| + |Y|}} = \frac{\frac{1}{2} \text{DSC}}{1 - \frac{1}{2} \text{DSC}} \\ &= \frac{\text{DSC}}{2 - \text{DSC}} \end{aligned}$$

This computational equivalence solidifies the relationship between the Jaccard Coefficient and DSC, suggesting they both measure over a similar characteristic in the context of segmentation. Given this, they do not supply independent information useful for differential model performance evaluation. Hence, our methodology uses the DSC as the primary metric instead of the Jaccard Coefficient to avoid redundancy.

### 7.1.3 Hausdorff Distance

While the quantity of accurate predictions (True Positives) undoubtedly contributes to successful segmentation, it is equally critical to scrutinize the shape of the generated mask, particularly in applications like organ segmentation. The Hausdorff Distance offers a comprehensive measure for evaluating the morphological similarity between the boundaries or contours of a predicted mask and ground truth.

Imagine two point sets  $A$  and  $B$  representing the contour coordinates. In this setting, the Hausdorff Distance manifests as:

$$\text{HD} = \max(h(A, B), h(B, A))$$

Where  $h(\cdot, \cdot)$  is defined as the directed Hausdorff distance, represented as

$$h(A, B) = \max_{a \in A} \min_{b \in B} d(a, b)$$

Here,  $d$  signifies a defined distance metric - for instance, the Euclidean or Manhattan distance. This measure essentially quantifies the greatest of all the closest distances from a point in one set to the other set. The Hausdorff Distance consequently assesses the maximum discrepancy between the two contours, providing valuable insight into the precision of the segmentation boundaries. Thus, This robust metric is a powerful tool for evaluating our model performance on contour prediction accuracy.

## 7.2 Evaluation Method

### 7.2.1 Employing Dice Similarity Coefficient for Qualitative Evaluation

The Dice Similarity Coefficient (DSC) is a standard for validating medical volume segmentations and measuring similarity across segmentation stages. We apply it consistently to our initial coarse weak masks, refined weak masks, and final performance, enabling tracking of our model's evolution over time.

Furthermore, by aligning our metric with prior work in this field, we ensure our results are directly comparable to earlier research. This facet not only bolsters the robustness of our findings but also situates our contributions within the broader scholarly discourse.

Hence, although seemingly straightforward, the strategic use of DSC plays a pivotal role in validating the efficacy of our segmentation method and facilitating meaningful comparisons with established literature.

### 7.2.2 Utilizing the t-Test for Evaluating Statistical Significance

In assessing improvements in our segmentation outcomes and weak label generation, we leverage the capabilities of a statistical method known as the

t-test. This test is a potent tool in distinguishing if the means of two groups, i.e. our baseline model performance and our proposed model performance, are statistically disparate.

We make the null hypothesis ( $H_0$ ) to suggest no significant difference between the means of these two groups. Conversely, the alternative hypothesis ( $H_1$ ) represents the situation where there exists a notable divergence in performance, indicative of an enhancement brought about by our new model.

Upon conducting the t-test by comparing the means of these two distinct groups and calculating the p-value, we are guided by conventional standards to reject  $H_0$  and accept  $H_1$  if the p-value falls below the typical significance threshold of 0.05. Such an event signifies a statistically robust improvement in our proposed model over the baseline model.

To summarize, the application of the t-test empowers us to conclusively attribute the witnessed improvements in our image segmentation results or weak-label generation not to random fluctuations but to substantial enhancements intrinsic to our developed model.

### 7.3 Evaluation Plan

A comprehensive evaluation plan has been conceived to ensure the fulfilment of our project objectives, meticulously assessing the performance at each pivotal milestone. The key components of our evaluation strategy involving the examination of the baseline model, refined masks, the fine-tuned model, and the execution of ablation studies are as follows:

1. **Baseline Model Evaluation:** We begin with a thorough evaluation of our baseline segmentation model, founded on the nnU-Net framework and reliant on the Simple Linear Iterative Clustering (SLIC) method for generating coarse-grained weak masks. Centred on transfer learning, this assessment phase will concentrate on the quality of the generated weak masks and the terminal ileum (T.I.) segmentation's initial performance, measured through the Dice Similarity Coefficient (DSC).
2. **Refined Mask Evaluation:** Upon successfully obtaining coarse-grained weak masks, the Segment Anything Model (SAM) is employed to yield refined masks with finer granularity. A comparative analysis will be conducted between the refined and coarse-grained masks, leveraging DSC and t-tests to examine their quality and effectiveness and validate the statistical significance of any observed improvements.
3. **Fine-Tuning and Target Model Evaluation:** With fully annotated data and refined weak masks, the model undergoes a fine-tuning process to attain our target segmentation model. This performance

evaluation stage will utilize DSC to assess the segmentation outcomes and t-tests to confirm the achieved improvement's statistical significance.

4. **Ablation studies:** Lastly, we aim to empirically validate the impact of using centerlines in enhancing SAM-driven weak mask generation. For this purpose, an ablation study will compare the quality of weak mask generation obtained from SAM with and without bounding boxes defined by the cents.

This robust evaluation blueprint ensures a methodical examination of our work, promising to validate the success of our project at every step and affirming its effective contribution to the advancement of terminal ileum segmentation.

# Chapter 8

## Results

This chapter is dedicated to the exposition and analysis of our experimental results. We shall commence by showcasing the performance of our model and meticulously comparing it against the baseline model derived from preceding work. The comparison will span two crucial stages - the generation of weak labels and the ultimate segmentation performance.

Beyond the comparative assessment, we thrust into statistical validation using the t-test. This step solidifies our evidence by testing the hypothesis concerning the improvement observed in our results.

Through this dual approach, with a comparative study augmented by rigorous statistical validation, we aim to furnish a comprehensive demonstration of the capabilities and advancements of our model over existing methods. We perform separate ablation studies to delve into the effect of potential key components on the segmentation performance. Collectively, these analyses form the backbone of our arguments, underpinning the significant contribution of our work in advancing state-of-the-art segmentation tasks.

### 8.1 Weak Label generation

A crucial component of our training pipeline is the process of weak label generation. This stage, marked by utilising centerline coordinates for creating a preliminary weak mask and subsequent enhancement through training with limited fully-connected data, plays a pivotal role in determining the final segmentation model performance.

With an emphasis on the decisive influence of the quality of weak labels, we present an in-depth comparison of the performance of our approach against the baseline model (Table 8.1). The results are examined in terms of the Dice Similarity Coefficient (DSC), with the details presented using the format  $\mu_i \pm \sigma_i$ , where  $\mu$  and  $\sigma$  denote the mean and variance of the DSC on test instances respectively.

Model	Average DSC (Axial)	Average DSC (Coronal)
Baseline	$0.5553 \pm 0.0755$	$0.5463 \pm 0.0986$
Our Method	<b><math>0.8084 \pm 0.0695</math></b>	<b><math>0.6941 \pm 0.0871</math></b>
(a) Average Case Comparison		
Model	Best DSC (Axial)	Best DSC (Coronal)
Baseline	0.6305	0.6559
Our Method	<b>0.8843</b>	<b>0.8251</b>
(b) Best Case Comparison		

Table 8.1: Weak Label Generation Comparison

In both the average and best-case scenarios, our method exhibits an appreciable edge over the baseline in terms of DSC values for axial and coronal images as shown in Tables 8.1a and 8.1b. It is noteworthy to highlight that our approach significantly outperforms the baseline derived from preceding work [9]. In terms of average performance, we observe uplifts of 45.58% and 27.05% for Axial T2 and Coronal images, respectively.

The sizable improvement is also evident when examining the best performance for each case type. With a remarkable increase of 40.24% for Axial T2 and a substantial 25.8% rise for Coronal T2 images, our approach convincingly demonstrates its effectiveness.

These results underline the efficacy of our method in generating high-quality weak labels that substantially enhance the final segmentation performance. These findings offer a promising perspective on the potential of our strategy to contribute meaningfully to advancements in terminal ileum segmentation tasks.

### 8.1.1 Visual Validation of Model Performance

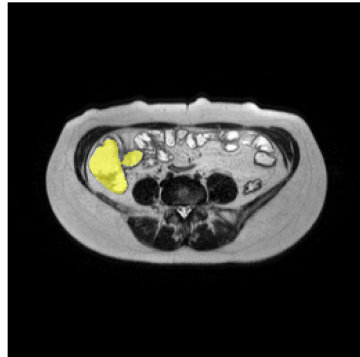
We offer a graphical representation of our model’s performance in Figure 8.1, providing a direct comparison between the generated weak masks and the corresponding ground truth annotations across both Coronal and Axial modalities.

Upon detailed observation, one can notice that the weak masks generated by our model align significantly well with the ground truth, as evidenced by the regions coloured yellow, which represent either the ground truth segmentation or the generated mask.

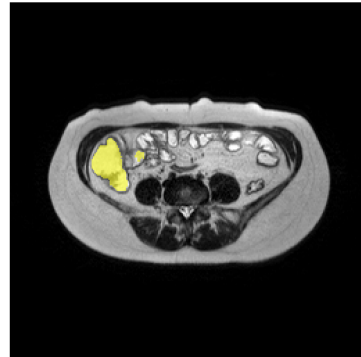
As portrayed in the paired images (Figs. 8.1a and 8.1b for Axial T2; Figs. 8.1c and 8.1d for Coronal T2), the substantial overlaps between our generated mask and the ground truth are noteworthy, with hardly discernible discrepancies.

This visual illustration accentuates the robustness of our model in generating highly accurate weak masks, thereby closely mirroring the ground

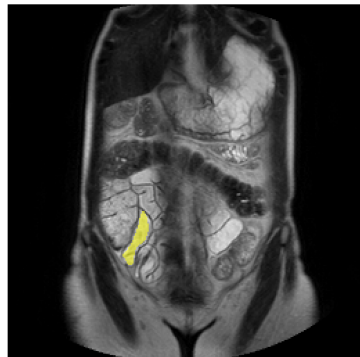
truth. Consequently, our model demonstrates remarkable potential in facilitating precise and dependable terminal ileum segmentation tasks, bridging the gap between machine-generated weak masks and human-annotated ground truths.



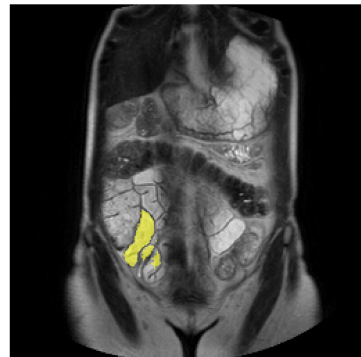
(a) Ground Truth on Axial T2



(b) Weak Mask on Axial T2



(c) Ground Truth on Coronal T2



(d) Weak Mask on Coronal T2

Figure 8.1: A Cross-Model Comparison between Ground Truth and Generated Weak Masks

### 8.1.2 Statistical Evaluation for Establishing Significance

In a bid to confirm the statistical significance of the enhancements realized through our approach, we employed the two-tailed t-test. Setting a significance level of 0.05, we sought a comparative study across modalities between the baseline and the outcomes generated through our technique.

It is important to note that the t-test utilized is an independent two-sample t-test as it takes into consideration results gathered separately from two distinct groups: the baseline results and those generated by our approach.

The table below presents a detailed view of the t-test outcomes:

Modality	<i>t</i> statistic	<i>p</i> value	significance level
Axial	3.9138	0.0029	0.05
Coronal	2.525	0.0355	0.05

These test results stand out because both cases' *p* values fall below the set significance level. This provides compelling evidence to dismiss our null hypothesis, confirming significant improvements in our weak label generation. Consequently, we can assertively state that our approach tangibly enhances the performances of the processes under study.

## 8.2 T.I. Segmentation

Completing our sophisticated two-phase training, we embarked on an evaluation phase for both the baseline and our model. The test set comprised 7 and 9 out of 38 and 48 human annotations for axial and coronal cases. The metrics employed for this evaluation were in line with the previously discussed Dice Similarity Coefficient (DSC), and the evaluation results are showcased in Table 8.2.

Model	Average DSC (Axial)	Average DSC (Coronal)
Baseline	$0.5691 \pm 0.1759$	$0.5824 \pm 0.1195$
Our Method	<b><math>0.7372 \pm 0.1692</math></b>	<b><math>0.6724 \pm 0.1174</math></b>

(a) Average Case Comparison		
Model	Best DSC (Axial)	Best DSC (Coronal)
Baseline	0.6573	0.6711
Our Method	<b>0.8975</b>	<b>0.8023</b>

(b) Best Case Comparison		
--------------------------	--	--

Table 8.2: Weak Label Generation Comparison

A comprehensive analysis of the results reveals that our method significantly outperforms the baseline regarding DSC values for both axial and coronal images. As Tables 8.2a and 8.2b portray, our model exhibits marked superiority over the baseline derived from prior work in routine and best-case performance scenarios.

Specifically, for average performance, our model delivers a robust improvement of 29.54% and 15.45% for Axial and Coronal T2 images, respec-

tively. Such substantial enhancements are also mirrored in optimal performance scenarios, reaping an impressive 36.54% and 19.55% increase for Axial and Coronal cases.

These rewarding outcomes vividly exemplify the substantial progression achieved over previous methodologies in terms of segmentation performance, reinforcing our commitment to continuously refine and improve our approaches in confronting the challenges posed by Crohn's disease.

### 8.2.1 Visual Validation of Model Performance

To illustrate the performance disparity between the baseline methodology and our refined approach, we provide a side-by-side visual comparison. This graphical representation ([Figure 8.2](#)) focuses on Axial T2 images, showcasing predictions generated by both the baseline model and our technique in contrast with the ground truth.

This visual analysis highlights the noticeable prevalence of false-positive classifications in the baseline prediction. Conversely, comparing our model and the ground truth reveals a significant alignment, barring minor discrepancies around the boundary contours. These findings visually affirm the advancements we have achieved in the T.I. segmentation, underscoring the superiority of our approach over the prior work.

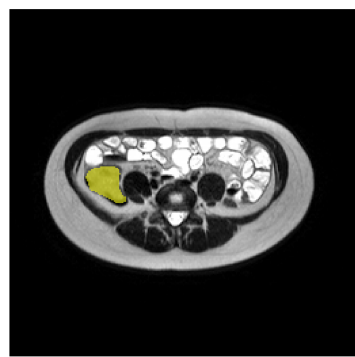
### 8.2.2 Statistical Evaluation for Establishing Significance

We conducted an additional t-test, maintaining the parameters specified earlier while assessing the generated weak labels. The table below delineates the decisive outcomes of these t-tests:

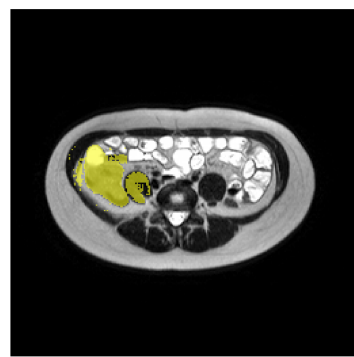
Modality	<i>t</i> statistic	<i>p</i> value	significance level
Axial	1.4492	0.1853	0.05
Coronal	1.3816	0.1860	0.05

Though we observed a considerable increase in the mean score and a comparable or even reduced standard deviation, the *p* values for both cases surpassed the 0.05 significance threshold. This outcome implies insufficient evidence to invalidate our null hypothesis or substantiate any improvements in the test results. Such contradiction is intriguing, particularly given the apparent disparity and enhancement between the baseline and our proposed approach.

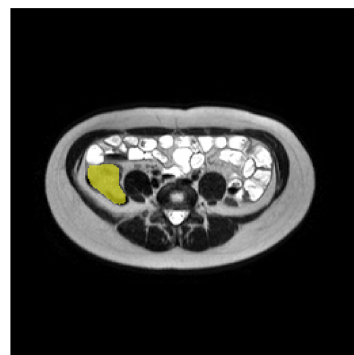
This finding potentially signifies an underpowered study, possibly due to the limited sample size. Even a seemingly substantial disparity in means may not yield statistical significance in such conditions. It might be beneficial to explore alternative statistical measures such as Cohen's *d* to gauge the magnitude of the improvement more accurately.



(a) Ground Truth



(b) Baseline Prediction



(c) Our Model Prediction

Figure 8.2: Comparative Segmentation Performance Analysis

### 8.3 Ablation Studies

Implementing the SAM-based pre-trained model has notably enhanced the quality of the generated weak masks. The training and fine-tuning of the SAM model, including weak label generation, leverage a centerline coordinate file that restricts the bounding box of the T.I. region. In this section, we conduct an ablation study to examine the impact of these centerlines, i.e. T.I. localisation—on the quality of weak labels and to inform potential strategies for subsequent training processes.

We initiated the experiment by refining two SAM models on an identical dataset, one integrated with the bounding box data derived from the centerline and the other devoid of such information. After fine-tuning, both models generated weak masks—one fully informed by the bounding box data and the other operating without it. We applied this methodology on Axial and Coronal images, and the resultant Dice Similarity Coefficient (DSC) was shown in [Table 8.3](#).

Modality	With localisation	No localisation
Axial	$0.8084 \pm 0.0695$	$0.0802 \pm 0.0115$
Coronal	$0.6941 \pm 0.0871$	$0.0524 \pm 0.0104$

Table 8.3: Impact of T.I. localisation

These results underscore the diminished performance of the SAM model in the absence of T.I. localisation. This observation ([Figure 8.3](#)) finds further validation in the following visual representation of Axial T2 images.

The visual results presented herein offer compelling evidence underlining the pivotal role of bounding boxes in generating high-quality weak masks or segmentations. This is not a mere enhancement but rather an essential ingredient to optimise the accuracy and quality of predictions. By observing the stark differences in the outcomes, with bounding box localisations leading to significantly superior results, it is clear that this element cannot be overlooked or underestimated in its impact.

In conclusion, our ablation study strongly suggests that localising the T.I. region via bounding box information significantly enhances the quality of weak labels generated by the SAM model. The Dice Similarity Coefficient (DSC) drastically declined when the models operated without centerline localisation, indicating a poor overlap between the predicted and actual results. This finding is consistent across both Axial and Coronal image modalities, as demonstrated by our t-tests and visually reinforced by the comparative images.

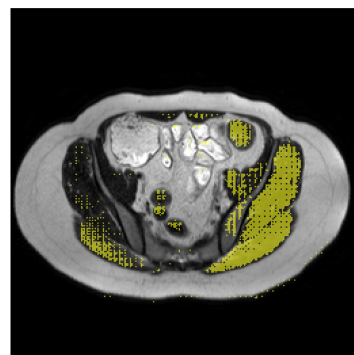
Moreover, our findings align with Huang et al. [21], further validating the importance of manual prompts, including points and bounding box information, to enhance the functionality of the SAM model. However, it is



(a) Ground Truth



(b) Prediction with T.I. localisation



(c) Prediction without T.I. localisation

Figure 8.3: Effect of T.I. Localisation on Mask Generation

worth noting that underperformances in the absence of T.I. localisation do not discount the potential of the SAM model. It only emphasises this specific input's crucial role in enhancing model performance.

As we pivot towards concluding our study and considering future work, it is clear that optimal utilisation of the SAM model for weak mask generation involves carefully considering these localisation factors. This understanding offers a solid foundation for future research efforts, allowing researchers to build upon these results, explore the model's full potential, and improve segmentation quality.

# Chapter 9

## Conclusion and Future Work

### 9.1 Conclusion

In this project, we presented our methodology, which leverages the strength of a refined weak label generation process and the capabilities of a pre-trained SAM model. The cornerstone of our approach lies in fine-tuning our model using comprehensive, fully annotated segmentation files. We subjected the resultant weak masks to a subsequent level of fine-tuning, thereby sculpting our target model.

The effectiveness of our proposed method is reflected in the marked enhancement of the Dice Similarity Coefficient (DSC) values. With an improvement of 29.53% and 15.45% across different modalities, the highest average DSC surged from 0.58 to a more favourable score of 0.73. This uplift signifies a substantial enhancement in the overlap between the predicted and actual segmentations, underscoring the efficacy of our technique in performing accurate segmentation tasks.

Further consolidating the credibility of our results, we performed graphical and statistical validation. This process ensured that the observed improvements were not the result of random variations but were a consequence of the systematic enhancements integrated into our model.

Additionally, we embarked on rigorous ablation studies to expound the contribution of each step in our refined method. During these explorations, the localisation of the terminal ileum (T.I.) within the bounding box emerged as a critical factor during the fine-tuning of the SAM model. The study reaffirmed the significance of maintaining attention to organ-specific regions for improved segmentation outcomes.

In conclusion, our work advances the frontiers of medical image segmentation by proposing an advanced method that amalgamates weak label generation with a pre-trained SAM model and strategic fine-tuning stages. Validated by substantial improvements and statistically confirmed results, our process establishes its potential for future medical imaging and diagnos-

tics applications.

## 9.2 Future Work

### Diffusion Models as Synthetic Data Generators

While our current model has demonstrated encouraging outcomes, the inherent limitation imposed by the scarcity of data and manual segmentations remains a constraint on the performance enhancement and generalizability in tackling Crohn’s disease through segmentation.

Recent studies, such as Lu et al. [29] and Xie et al. [30], have highlighted the proficiency of diffusion models in synthesising Magnetic Resonance (MR) Images effectively. We see a promising new research trajectory to explore in this burgeoning field.

Diffusion models can be instrumental in fabricating or reconstructing synthetic abdominal MRI scans. This approach circumvents the need for extensive manual segmentations, which often entail significant temporal and financial costs.

By harnessing the power of diffusion models, we open avenues for creating a robust, diversified data corpus that eliminates the need for resource-intensive manual input and paves the way for advanced explorations in tackling abdominal imaging challenges.

Infusing synthetic data can enrich the diversity and volume of available data, providing a more robust, comprehensive substrate for training our model. Coupled with our potent methodology in proxy training, this offers a unique vantage point to push the boundaries of segmentation performance in tackling Crohn’s disease.

As a natural extension of our present work, leveraging diffusion models for synthetic data generation can significantly address data limitations and propel the efficacy of deep learning algorithms in diagnosing and treating Crohn’s disease to unprecedented levels.

### Abnormal T.I. Tissues Detection

Our research has laid a solid groundwork with a binary segmentation model for the terminal ileum (T.I.) in T2-weighted MRI images, displaying exceptional segmentation outcomes - a pivotal stride towards improved diagnostics.

Looking ahead, we aim to extend this research by devising sophisticated multi-class segmentation models capable of distinguishing between normal and abnormal T.I. tissues based on prior work [9]. The remarkable performance of our current binary segmentation model sets an encouraging precedent for this upcoming venture.

The advent of a multi-class segmentation model will significantly heighten diagnostic precision by identifying varying pathologies within the T.I., thereby paving the way for tailored treatment plans. This advance will also provide a crucial understanding of disease progression by shedding light on the characteristics and severity of tissue abnormalities.

Implementation of such a multi-class model poses challenges, including dataset class imbalance and the need for intricate training processes. However, strategies like data augmentation, transfer learning, or innovative loss functions can be explored to alleviate these challenges.

The success of this future endeavour bears profound implications for refining early detection and treatment planning for Crohn's patients and enhancing their quality of life. This avenue of research harbours extensive potential for managing Crohn's disease and potentially other gastrointestinal disorders exhibiting similar radiographic patterns.

### **Human in the Loop**

While deep learning techniques can automate the process of segmentation and analysis, incorporating human expertise can significantly improve the reliability and effectiveness of the model. Future work could explore "human-in-the-loop" methods where medical experts provide real-time feedback during the training process. This could allow for developing more sophisticated models that better understand and mimic expert knowledge in diagnosing and treating Crohn's disease.

### **Real-Time Segmentation**

In medical applications, real-time processing is critical for timely diagnosis and treatment. A future research objective could be devoted to optimizing our model performance for real-time segmentation. This would be particularly beneficial during surgical procedures or emergency scenarios where clinicians require immediate information. Adapting our model to operate effectively in real-time conditions will necessitate focused research on computational efficiency and speed optimization.

Collectively, these future pursuits promise to enhance the potency of deep learning algorithms in mastering the challenging task of diagnosing and combating Crohn's disease, moving us closer to more efficient patient outcomes and healthcare services.

# Bibliography

- [1] Daniel C Baumgart and William J Sandborn. Crohn’s disease. *The Lancet*, 380(9853):1590–1605, 2012.
- [2] NHS. Crohn’s disease - nhs. URL <https://www.nhs.uk/conditions/crohns-disease/>.
- [3] Centers for Disease Control and Prevention. What is inflammatory bowel disease? (ibd) | ibd. URL <https://www.cdc.gov/ibd/what-is-IBD.htm>.
- [4] The human digestive system. <https://crohnsandcolitis.org.uk/media/ftsl0iea/digestion-graphic.jpg>. (Accessed on 06/13/2023).
- [5] University of Nottingham. Rates of crohn’s and colitis have been vastly underestimated for decades, says new study. URL <https://www.nottingham.ac.uk/news/rates-of-crohns-and-colitis-have-been-vastly-underestimated-for-decades-says-new-study>.
- [6] Gautier Hoarau, PK Mukherjee, C Gower-Rousseau, C Hager, J Chandra, MA Retuerto, Christel Neut, Séverine Vermeire, J Clemente, Jean-Frederic Colombel, et al. Bacteriome and mycobiome interactions underscore microbial dysbiosis in familial crohn’s disease. *MBio*, 7(5):e01250–16, 2016.
- [7] Joseph D Feuerstein, Edith Y Ho, Eugenia Shmidt, Harminder Singh, Yngve Falck-Ytter, Shanaz Sultan, Jonathan P Terdiman, Shahnaz Sultan, Benjamin L Cohen, Karen Chachu, et al. Aga clinical practice guidelines on the medical management of moderate to severe luminal and perianal fistulizing crohn’s disease. *Gastroenterology*, 160(7):2496–2508, 2021.
- [8] Robert Holland, Uday Patel, Phillip Lung, Elisa Chotzoglou, and Bernhard Kainz. Automatic detection of bowel disease with residual networks. In *International Workshop on PReditive Intelligence In MEdicine*, pages 151–159. Springer, 2019.

- [9] Ali Abidi. Tackling crohn’s disease using deep learning. Master’s thesis, Imperial College London, 2022.
- [10] Fabian Isensee, Paul F Jaeger, Simon AA Kohl, Jens Petersen, and Klaus H Maier-Hein. nnu-net: a self-configuring method for deep learning-based biomedical image segmentation. *Nature methods*, 18(2):203–211, 2021.
- [11] Jong-Hwan Jang, Tae Young Kim, and Dukyong Yoon. Effectiveness of transfer learning for deep learning-based electrocardiogram analysis. *Healthcare informatics research*, 27(1):19–28, 2021.
- [12] Alexander Kirillov, Eric Mintun, Nikhila Ravi, Hanzi Mao, Chloe Rolland, Laura Gustafson, Tete Xiao, Spencer Whitehead, Alexander C. Berg, Wan-Yen Lo, Piotr Dollár, and Ross Girshick. Segment anything. *arXiv:2304.02643*, 2023.
- [13] Ben Glocker. Image segmentation - machine learning for imaging course, 2023.
- [14] Rolf Adams and Leanne Bischof. Seeded region growing. *IEEE Transactions on pattern analysis and machine intelligence*, 16(6):641–647, 1994.
- [15] Olaf Ronneberger, Philipp Fischer, and Thomas Brox. U-net: Convolutional networks for biomedical image segmentation. In *International Conference on Medical image computing and computer-assisted intervention*, pages 234–241. Springer, 2015.
- [16] Jonathan Long, Evan Shelhamer, and Trevor Darrell. Fully convolutional networks for semantic segmentation. In *Proceedings of the IEEE conference on computer vision and pattern recognition*, pages 3431–3440, 2015.
- [17] Fabian Isensee, Jens Petersen, Andre Klein, David Zimmerer, Paul F Jaeger, Simon Kohl, Jakob Wasserthal, Gregor Koehler, Tobias Norajittra, Sebastian Wirkert, et al. nnu-net: Self-adapting framework for u-net-based medical image segmentation. *arXiv preprint arXiv:1809.10486*, 2018.
- [18] Fabian Isensee, Jens Petersen, Simon AA Kohl, Paul F Jäger, and Klaus H Maier-Hein. nnu-net: Breaking the spell on successful medical image segmentation. *arXiv preprint arXiv:1904.08128*, 1(1-8):2, 2019.
- [19] Radhakrishna Achanta, Appu Shaji, Kevin Smith, Aurelien Lucchi, Pascal Fua, and Sabine Süsstrunk. Slic superpixels. Technical report, 2010.
- [20] Jun Ma and Bo Wang. Segment anything in medical images. *arXiv preprint arXiv:2304.12306*, 2023.

- [21] Yuhao Huang, Xin Yang, Lian Liu, Han Zhou, Ao Chang, Xinrui Zhou, Rusi Chen, Junxuan Yu, Jiongquan Chen, Chaoyu Chen, Haozhe Chi, Xindi Hu, Deng-Ping Fan, Fajin Dong, and Dong Ni. Segment anything model for medical images?, 2023.
- [22] Dwarikanath Mahapatra, Peter J Schüffler, Jeroen AW Tielbeek, Jesica C Makanyanga, Jaap Stoker, Stuart A Taylor, Franciscus M Vos, and Joachim M Buhmann. Automatic detection and segmentation of crohn’s disease tissues from abdominal mri. *IEEE transactions on medical imaging*, 32(12):2332–2347, 2013.
- [23] Kaiming He, Xiangyu Zhang, Shaoqing Ren, and Jian Sun. Deep residual learning for image recognition. In *Proceedings of the IEEE conference on computer vision and pattern recognition*, pages 770–778, 2016.
- [24] Jo Schlemper, Ozan Oktay, Michiel Schaap, Mattias Heinrich, Bernhard Kainz, Ben Glocker, and Daniel Rueckert. Attention gated networks: Learning to leverage salient regions in medical images. *Medical image analysis*, 53:197–207, 2019.
- [25] Jordi Rimola, Sonia Rodríguez, Orlando García-Bosch, Ingrid Ordás, Edgar Ayala, Montserrat Aceituno, Maria Pellisé, Carmen Ayuso, Elena Ricart, Lluís Donoso, et al. Magnetic resonance for assessment of disease activity and severity in ileocolonic crohn’s disease. *Gut*, 58(8):1113–1120, 2009.
- [26] Binu E Enchakalody, Brianna Henderson, Stewart C Wang, Grace L Su, Ashish P Wasnik, Mahmoud M Al-Hawary, and Ryan W Stidham. Machine learning methods to predict presence of intestine damage in patients with crohn’s disease. In *Medical Imaging 2020: Computer-Aided Diagnosis*, volume 11314, pages 742–753. SPIE, 2020.
- [27] Michal Drozdzal, Eugene Vorontsov, Gabriel Chartrand, Samuel Kadouri, and Chris Pal. The importance of skip connections in biomedical image segmentation. In *International Workshop on Deep Learning in Medical Image Analysis, International Workshop on Large-Scale Annotation of Biomedical Data and Expert Label Synthesis*, pages 179–187. Springer, 2016.
- [28] lecture\_slides\_lec6.pdf. [http://www.cs.toronto.edu/~tijmen/csc321/slides/lecture\\_slides\\_lec6.pdf](http://www.cs.toronto.edu/~tijmen/csc321/slides/lecture_slides_lec6.pdf). (Accessed on 06/18/2023).
- [29] Yizhuo Lu, Changde Du, Dianpeng Wang, and Huiuguang He. Minddiffuser: Controlled image reconstruction from human brain activity with semantic and structural diffusion. *arXiv preprint arXiv:2303.14139*, 2023.

- [30] Taofeng Xie, Chentao Cao, Zhuoxu Cui, Yu Guo, Caiying Wu, Xuemei Wang, Qingneng Li, Zhanli Hu, Tao Sun, Ziru Sang, et al. Synthesizing pet images from high-field and ultra-high-field mr images using joint diffusion attention model. *arXiv preprint arXiv:2305.03901*, 2023.